

Fracture induced anisotropy in viscoelastic media

UNLP, 11 Octubre de 2012

- **Fractures** are common in the earth's crust due to different factors, for instance, tectonic stresses and natural or artificial hydraulic fracturing caused by a pressurized fluid.
- **Seismic wave propagation** through **fractures and cracks** is an important subject in exploration and production geophysics, earthquake seismology and mining.
- **Fractures** constitute the sources of earthquakes, and hydrocarbon and geothermal reservoirs are mainly composed of **fractured rocks**.

- Modeling fractures requires a suitable interface model. Schoenberg (JASA (1980), GP (1983)) proposed the so-called linear-slip boundary condition model (LSBC), based on the discontinuity of the displacement across the fractures. (Schoenberg's model).
- A generalization of the (LSBC) (Carcione, JGR (1996)) states that across a fracture stress components are proportional to the displacement and velocity discontinuities through the specific stiffnesses and viscosities, respectively.

Fractured media. III

- Displacement discontinuities **conserve energy**, while velocity discontinuities generate **energy loss** at the fractures. The specific viscosity accounts for the presence of a **liquid** under saturated conditions, introducing a viscous coupling between both sides of a fracture.
- Schoenberg's theory predicts that **a dense set of parallel plane fractures** behaves as a **Transversely Isotropic Viscoelastic (TIV) medium** if the dominant wavelength of the traveling waves is much larger than the distance between the fractures.

Fractured media. IV

- Schoenberg's model has never been simulated with a numerical method.
- In the context of Numerical rock physics we present a novel numerical solver that can be used in more general situations.
- To determine the complex stiffness coefficients of the equivalent TIV medium, we solve a set of boundary value problems (BVP's) for the wave equation of motion in the frequency-domain using the finite-element method (FEM).
- The BVP's represent harmonic tests at a finite number of frequencies on a sample having a dense set of fractures, modeled using the LSBC.

The equivalent TIV medium. I

Consider a **viscoelastic isotropic background medium** having a **set of parallel (horizontal) fractures** and its description in the space-frequency domain.

\mathbf{u} , $\mathbf{e}(\mathbf{u})$, $\boldsymbol{\sigma}(\mathbf{u})$: frequency domain displacement vector, strain and stress tensors of the background medium at the mesoscale.

The **stress-strain relations** and **equations of motion**:

$$\sigma_{jk}(\mathbf{u}) = \lambda \delta_{jk} \nabla \cdot \mathbf{u} + 2\mu e_{jk}(\mathbf{u})$$

$$\rho \omega^2 \mathbf{u}(x, z, \omega) + \nabla \cdot \boldsymbol{\sigma}[\mathbf{u}(x, z, \omega)] = 0$$

δ_{jk} : Kroenecker delta λ, μ : complex Lamé constants ρ : mass density.

The equivalent TIV medium. II

x_1 and x_3 : horizontal and vertical coordinates, respectively.

When a **dense set of parallel fractures** is present, the medium behaves as a **TIV medium** with x_3 -axis of symmetry at long wavelengths (macroscale).

$\boldsymbol{\tau}$, $\boldsymbol{\epsilon}$: stress and strain tensors of the equivalent TIV medium at the macroscale. **Stress-strain relations at the macroscale:**

$$\tau_{11}(\mathbf{u}) = p_{11} \epsilon_{11}(\mathbf{u}) + p_{12} \epsilon_{22}(\mathbf{u}) + p_{13} \epsilon_{33}(\mathbf{u}),$$

$$\tau_{22}(\mathbf{u}) = p_{12} \epsilon_{11}(\mathbf{u}) + p_{11} \epsilon_{22}(\mathbf{u}) + p_{13} \epsilon_{33}(\mathbf{u}),$$

$$\tau_{33}(\mathbf{u}) = p_{13} \epsilon_{11}(\mathbf{u}) + p_{13} \epsilon_{22}(\mathbf{u}) + p_{33} \epsilon_{33}(\mathbf{u}),$$

$$\tau_{23}(\mathbf{u}) = 2 p_{55} \epsilon_{23}(\mathbf{u}),$$

$$\tau_{13}(\mathbf{u}) = 2 p_{55} \epsilon_{13}(\mathbf{u}), \quad \tau_{12}(\mathbf{u}) = 2 p_{66} \epsilon_{12}(\mathbf{u}).$$

Schoenberg's theory predicts that if the background medium is homogeneous, the stiffnesses p_{IJ} 's are given by

$$p_{11} = p_{22} = E - \lambda^2 Z_N c_N, \quad p_{12} = \lambda - \lambda^2 Z_N c_N \quad p_{13} = \lambda c_N, \\ p_{33} = E c_N, \quad p_{55} = \mu c_T, \quad p_{66} = \mu.$$

where

$$c_N = (1 + E Z_N)^{-1} \quad \text{and} \quad c_T = (1 + \mu Z_T)^{-1},$$

Z_N and Z_T : normal and tangential complex compliances of the fractures
 $E = \lambda + 2\mu$.

The equivalent TIV medium. IV

The **theory** assumes that that distance between fractures is much smaller than the wavelength of the signal and that the **boundary condition is the same for all the fractures**.

Moreover, the theory assumes that the **fracture distance is constant**.

The **numerical solver** may consider an inhomogeneous background medium, unequal fracture distances and dissimilar boundary conditions at the fractures surfaces.

The p_{IJ} 's are the complex and frequency-dependent stiffnesses to be determined numerically with the harmonic experiments.

Determination of the stiffness components p_{IJ}

$\Omega = (0, D)^2$: **a square sample of boundary** $\Gamma = \Gamma^L \cup \Gamma^R \cup \Gamma^B \cup \Gamma^T$,
where

$$\begin{aligned}\Gamma^L &= \{(x, z) \in \Gamma : x = 0\}, & \Gamma^R &= \{(x, z) \in \Gamma : x = D\}, \\ \Gamma^B &= \{(x, z) \in \Gamma : z = 0\}, & \Gamma^T &= \{(x, z) \in \Gamma : z = D\}.\end{aligned}$$

$\Gamma^{(f,l)}, l = 1, \dots, J^{(f)}$: **a set of $J^{(f)}$ horizontal fractures each one of length D in our domain Ω .**

This set of fractures divides Ω in a set of nonoverlapping rectangles $R^{(l)}, l = 1, \dots, J^f + 1$, so that

$$\Omega = \cup_{l=1}^{J^{(f)}+1} R^{(l)}.$$

Boundary conditions at the fractures. I

Consider a fracture $\Gamma^{(f,l)}$ and the two rectangles $R^{(l)}$ and $R^{(l+1)}$ having as a common side $\Gamma^{(f,l)}$.

$\nu_{l,l+1}, \chi_{l,l+1}$: the unit outer normal and a unit tangent (oriented counterclockwise) on $\Gamma^{(f,l)}$ from $R^{(l)}$ to $R^{(l+1)}$, such that $\{\nu_{l,l+1}, \chi_{l,l+1}\}$ is an orthonormal system on $\Gamma^{(f,l)}$.

Set $\mathbf{u}^{(l)} = \mathbf{u}|_{R^{(l)}}$: restriction of \mathbf{u} to $R^{(l)}$, and let

$$[\mathbf{u}] = (\mathbf{u}^{(l)} - \mathbf{u}^{(l+1)})|_{\Gamma^{(f,l)}}$$

denote the **jump of \mathbf{u} at $\Gamma^{(f,l)}$**

Boundary conditions at the fractures. II

The boundary conditions (B.C.) at the fractures $\Gamma^{(f,l)}$ are **the stress continuity** and the condition that **stress components be proportional to the displacement and velocity discontinuities** through **specific stiffnesses and viscosities**, respectively. Thus,

$$\sigma(u^{(l)})\nu_{l,l+1} = \sigma(u^{(l+1)})\nu_{l,l+1} \quad \Gamma^{(f,l)},$$

$$\sigma(u^{(l)})\nu_{l,l+1} \cdot \nu_{l,l+1} = (LZ_N^l)^{-1}[u] \cdot \nu_{l,l+1}$$

$$\sigma(u^{(l)})\nu_{l,l+1} \cdot \chi_{l,l+1} = (LZ_T^l)^{-1}[u] \cdot \chi_{l,l+1} \quad \Gamma^{(f,l)}, \quad l = 1, \dots, J^{(f)}.$$

L : average distance between the fractures

The **compliances** Z (Z_N or Z_T) are complex and frequency-dependent and can be expressed as

$$Z^{-1} = L(\kappa + i\omega\eta),$$

where κ is a specific stiffness and η is a specific viscosity, having dimensions of stiffness and viscosity per unit length, respectively.

For p_{33} we solve the wave equation in Ω using the fracture B. C.'s with the additional B. C.'s

$$\sigma(u)\nu \cdot \nu = -\Delta P, \quad \Gamma^T, \quad (1)$$

$$\sigma(u)\nu \cdot \chi = 0, \quad \Gamma, \quad (2)$$

$$u \cdot \nu = 0, \quad \Gamma^L \cup \Gamma^R \cup \Gamma^B. \quad (3)$$

In this experiment $\epsilon_{11}(u) = \epsilon_{22}(u) = 0$.

Determination of the stiffness components p_{IJ} . II

Denoting by V the original volume of the sample, its (complex) oscillatory volume change, $\Delta V(\omega)$, we note that in the quasistatic case

$$\frac{\Delta V(\omega)}{V} = -\frac{\Delta P}{p_{33}(\omega)},$$

The computed average vertical displacement $u_3^{s,T}(\omega)$ suffered by the boundary Γ^T allows us to use the estimate

$$\Delta V(\omega) \approx Du_3^{s,T}(\omega),$$

from where we can determine $p_{33}(\omega)$.

Determination of the stiffness components p_{IJ} . III

For p_{11} we solve the wave equation with the fracture B. C.'s and the additional B. C.'s

$$\sigma(u) \cdot \nu \cdot \nu = -\Delta P, \quad \Gamma^R,$$

$$\sigma(u) \cdot \nu \cdot \chi = 0, \quad \Gamma,$$

$$u \cdot \nu = 0, \quad \Gamma^L \cup \Gamma^B \cup \Gamma^T.$$

In this experiment, $\epsilon_{33} = \epsilon_{22} = 0$ and this experiment determines p_{11} computing the volume change in the same way indicated for p_{33} .

For p_{55} we solve the wave equation with the fracture B. C.'s and the additional B. C.'s

$$\begin{aligned}\boldsymbol{\sigma} \cdot \boldsymbol{\chi} &= \mathbf{g}, \quad \Gamma^T \cup \Gamma^L \cup \Gamma^R, \\ \mathbf{u} &= 0, \quad \Gamma^B,\end{aligned}$$

where

$$\mathbf{g} = \begin{cases} (0, \Delta G), & \Gamma^L, \\ (0, -\Delta G), & \Gamma^R, \\ (\Delta G, 0), & \Gamma^T. \end{cases}$$

Determination of the stiffness components p_{IJ} . V

Let $\theta(\omega)$: angle between the original positions of the lateral boundaries and the location after applying the shear stresses.

To estimate $\theta(\omega)$, we compute the average horizontal displacement $u_1^T(\omega)$ at the boundary Γ^T and use that

$$\tan[\theta(\omega)] \approx u_1^T(\omega)/D.$$

Thus, **the change in shape of the rock sample** allow us to determine $p_{55}(\omega)$ from the relation (Kolsky, 1963)

$$\tan[\theta(\omega)] = \frac{\Delta G}{p_{55}(\omega)}.$$

For p_{13} we solve the wave equation with the fracture B. C.'s and the additional B. C.'s

$$\sigma(u) \cdot \nu \cdot \nu = -\Delta P, \quad \Gamma^R \cup \Gamma^T,$$

$$\sigma(u) \cdot \nu \cdot \chi = 0, \quad \Gamma,$$

$$u \cdot \nu = 0, \quad \Gamma^L \cup \Gamma^B.$$

In this experiment $\epsilon_{22} = 0$, and from the stress-strain relations at the macroscale we get

Determination of the stiffness components p_{IJ} . VII

$$\tau_{11} = p_{11}\epsilon_{11} + p_{13}\epsilon_{33},$$

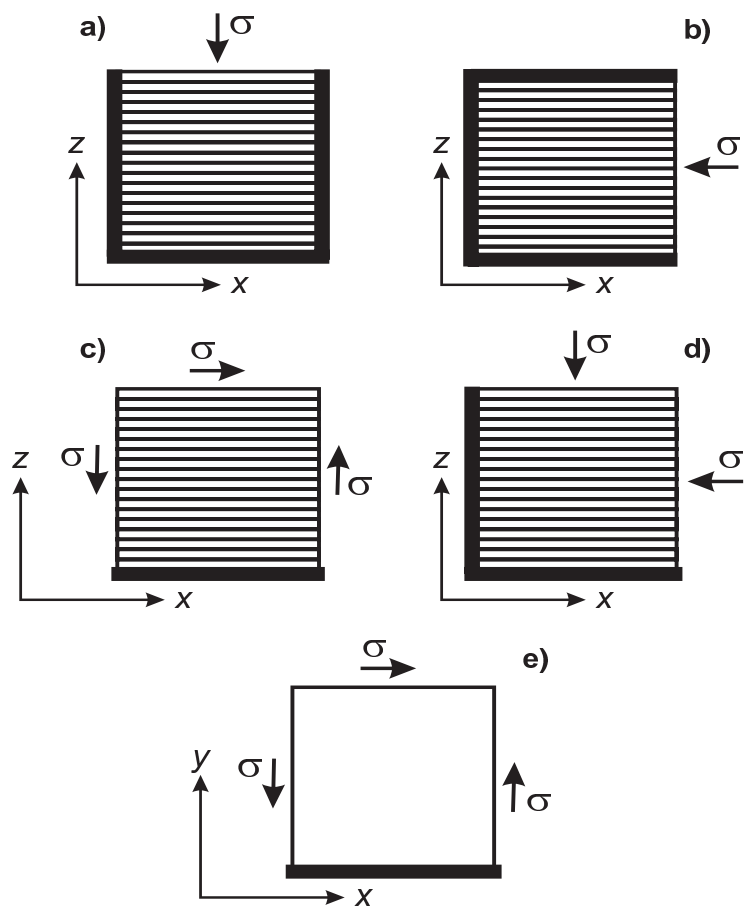
$$\tau_{33} = p_{13}\epsilon_{11} + p_{33}\epsilon_{33},$$

$\epsilon_{11}, \epsilon_{33}$: macroscopic strain components at the right lateral side and top side of the sample, respectively.

Then using that $\tau_{11} = \tau_{33} = -\Delta P$ we obtain

$$p_{13}(\omega) = \frac{p_{11}\epsilon_{11} - p_{33}\epsilon_{33}}{\epsilon_{11} - \epsilon_{33}}.$$

Schematic representation of the oscillatory compressibility and shear tests in Ω



A variational formulation

Test space for $\mathbf{p}_{33}(\omega)$:

$$\mathcal{W}_{33}(\Omega) = \{v \in [L^2(\Omega)]^2 : v|_{R^{(l)}} \in [H^1(R^{(l)})]^2, v \cdot \nu = 0 \text{ on } \Gamma^L \cup \Gamma^R \cup \Gamma^B\},$$

To determine $\mathbf{p}_{33}(\omega)$: find $\mathbf{u}^{(33)} \in \mathcal{W}_{33}(\Omega)$ such that:

$$\begin{aligned} & -\omega^2(u, v) + \sum_{l=1}^{J(f)+1} \sum_{s,t=1,3} (\sigma_{st}(u), \epsilon_{st}(v))_{R^{(l)}} \\ & + \sum_{l=1}^{J(f)} \left[\left\langle [LZ_N^{(l)}]^{-1}[u]_3, [v]_3 \right\rangle_{\Gamma(f,l)} + \left\langle [LZ_T^{(l)}]^{-1}[u]_1, [v]_1 \right\rangle_{\Gamma(f,l)} \right] \\ & = -\langle \Delta P, v \cdot \nu \rangle_{\Gamma^T}, \quad \forall v \in \mathcal{W}_{33}(\Omega). \end{aligned}$$

Similar formulations hold for the other \mathbf{p}_{IJ} 's

Finite element implementation

The FE variational formulation uses **bilinear elements** to compute approximate solution of the BVP.

The **error** is of the order of **h** in the **L^2 -norm** and of the order of **$h^{1/2}$** both in the **interior energy norm** and in the **L^2 -norm** on the set of fractures, where **h** is the diameter of the elements.

Numerical experiments.

We consider the data provided by the laboratory experiments of Chichinina et al. (TPM, 2009). The background medium is isotropic with $\lambda = 10$ GPa, $\mu = 3.9$ GPa and $\rho = 2300$ kg/m³.

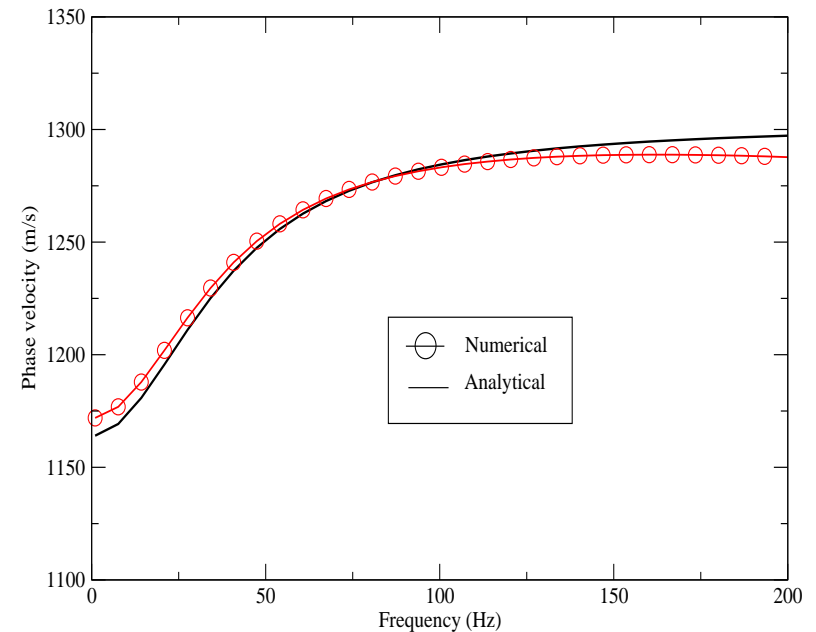
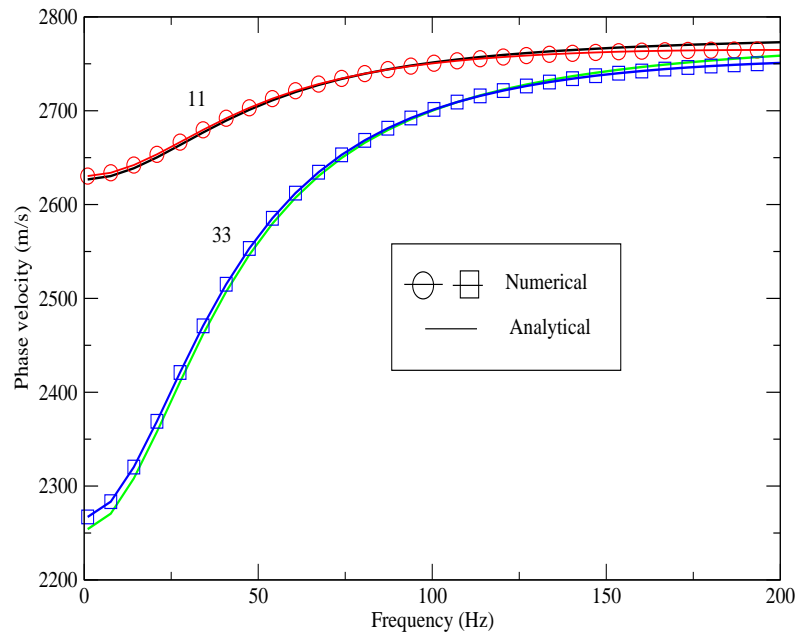
The simulations to determine the \mathbf{p}_{IJ} 's have 29 equally spaced fractures, fracture distance $L = 1$ cm, grid spacing $h = 0.5$ cm and a frequency $f_0 = 25$ Hz, employing a 60×60 mesh.

Experimental values of \mathbf{Z}_N and \mathbf{Z}_T for wet fractures scaled to seismic frequencies:

$$\mathbf{Z}_N^{-1} = [34 + i(f/f_0) \ 24.7] \text{ GPa} \quad \mathbf{Z}_T^{-1} = [15.5 + i(f/f_0) \ 11.3] \text{ GPa}$$

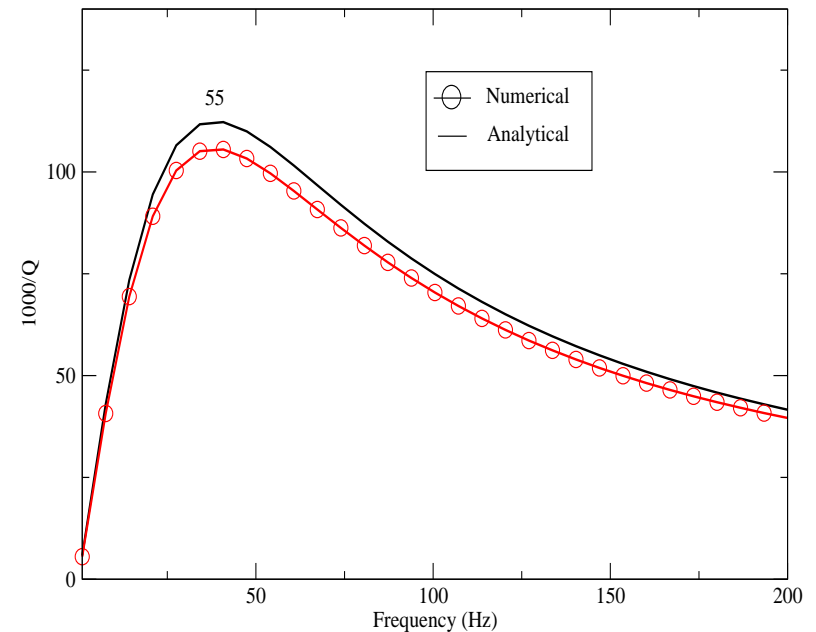
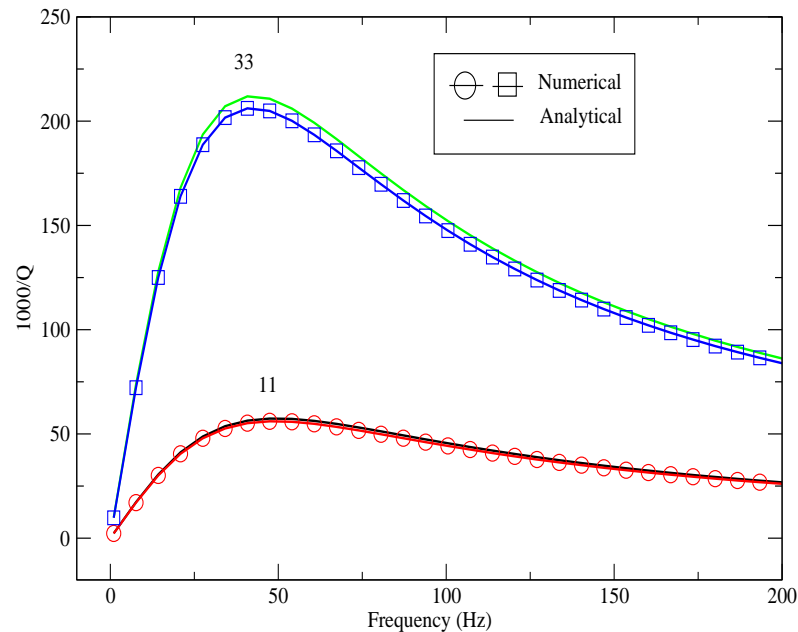
Determination of reliable fracture parameters needs measurements at the seismic range (experimental data was obtained at 100 kHz).

Validation of the FE method. Phase velocities as function of frequency for wet fr



“11” and “33” refer to the qP wave along and perpendicular to the fracture plane. “55” refers to the qS wave perpendicular to the fracture plane. A very good fit is observed. qP waves along the fracture plane (“11”) travel faster than qP waves travelling perpendicular to the fractures (“33”).

Validation of the FE method. Dissipation factor as function of frequency for wet



“11” and “33” refer to the qP wave along and perpendicular to the fracture plane. “55” and “66” refer to the qS and SH waves perpendicular and along the fracture plane. The SH wave is lossless. A very good fit is observed. qP waves along the fracture plane (“11”) suffer lower attenuation than qP waves travelling perpendicular to the fractures (“33”).

Fractures at varying pore fluid pressure .

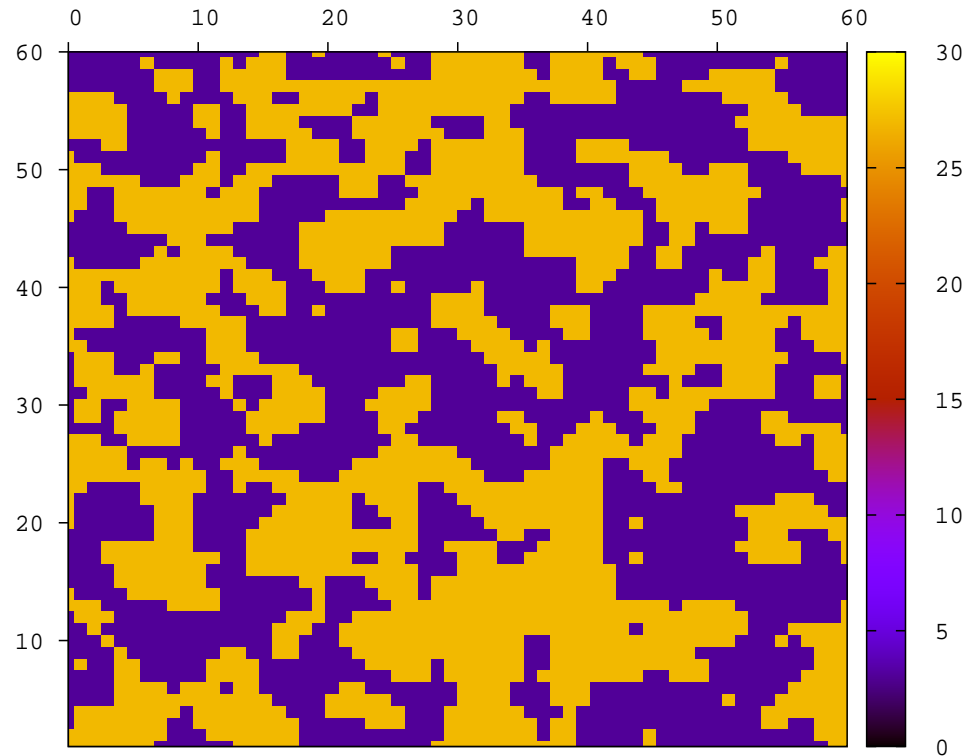
Daley et al. (GPY, 2006) suggest to take high values of fracture compliance at low normal **effective stress** $\sigma = p_c - p_p$, where p_c is the confining pressure and p_p the pore pressure.

For a constant $p_c = 30$ MPa, we consider two pore pressures 5 MPa and 25 MPa, normal and overpressure values, respectively. Using their model, we obtain, at 25 Hz,

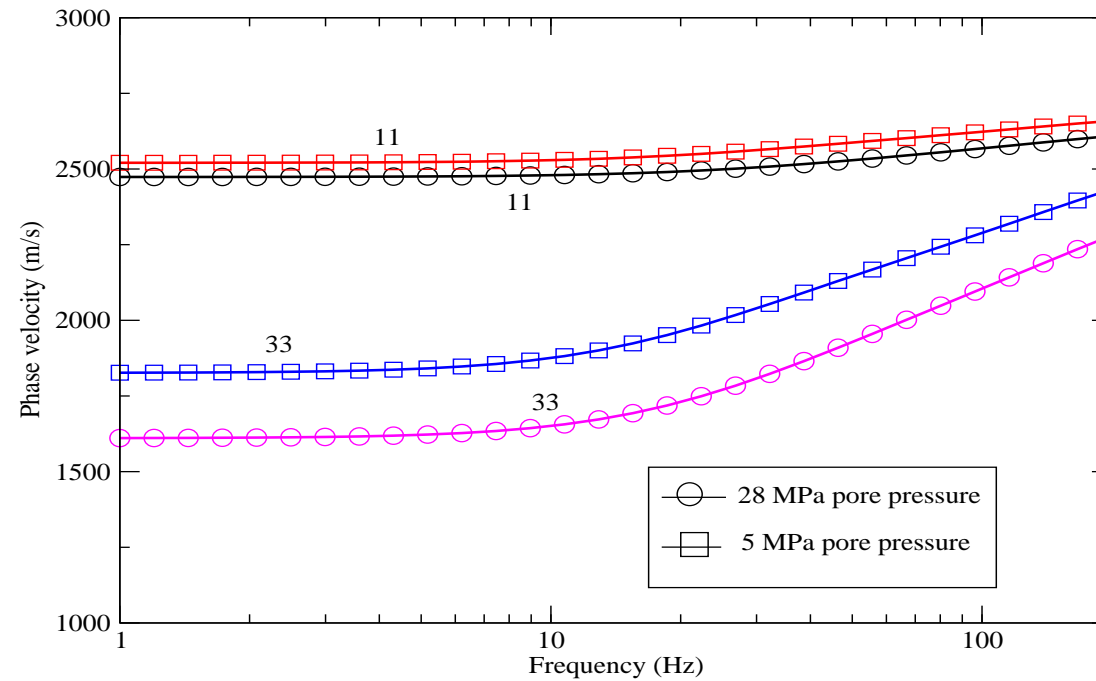
$$\begin{aligned} p_p = 5 \text{ MPa}, \quad Z_N^{-1} &= (23.1 + 5.9i) \text{ GPa}, \quad Z_T^{-1} = (75 + 9.4i) \text{ GPa}, \\ p_p = 28 \text{ MPa}, \quad Z_N^{-1} &= (14.4 + 3.6i) \text{ GPa}, \quad Z_T^{-1} = (21 + 2.6i) \text{ GPa}, \end{aligned}$$

We consider a set of equispaced fractures with $L = 1$ cm and 80 % binary fractal variations of Z_N and Z_T around these mean values.

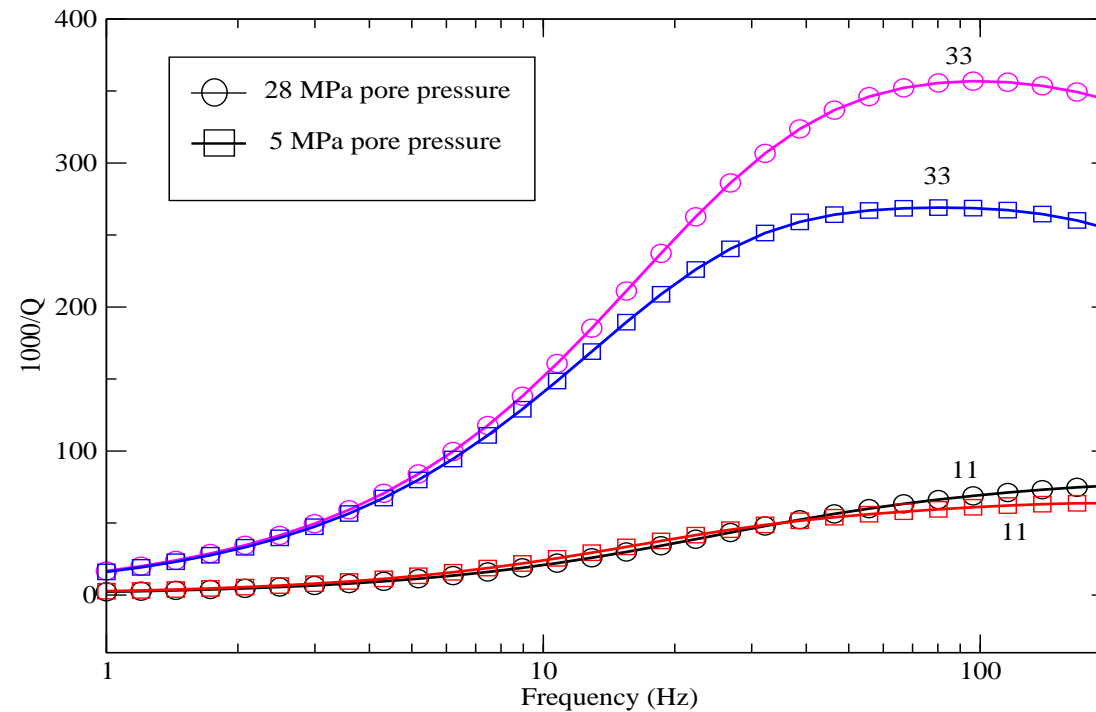
Real part of fractal Z_N^{-1} at pore pressure 28 MPa.



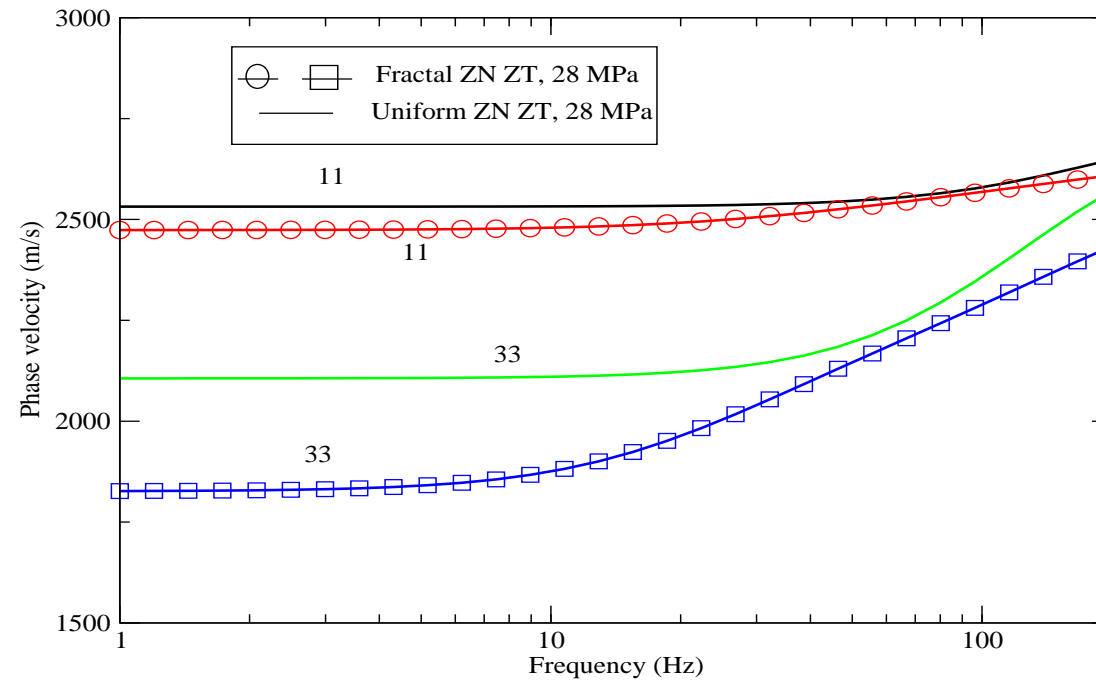
80 % binary fractal variations of Z_N around the mean value 23.1 GPa



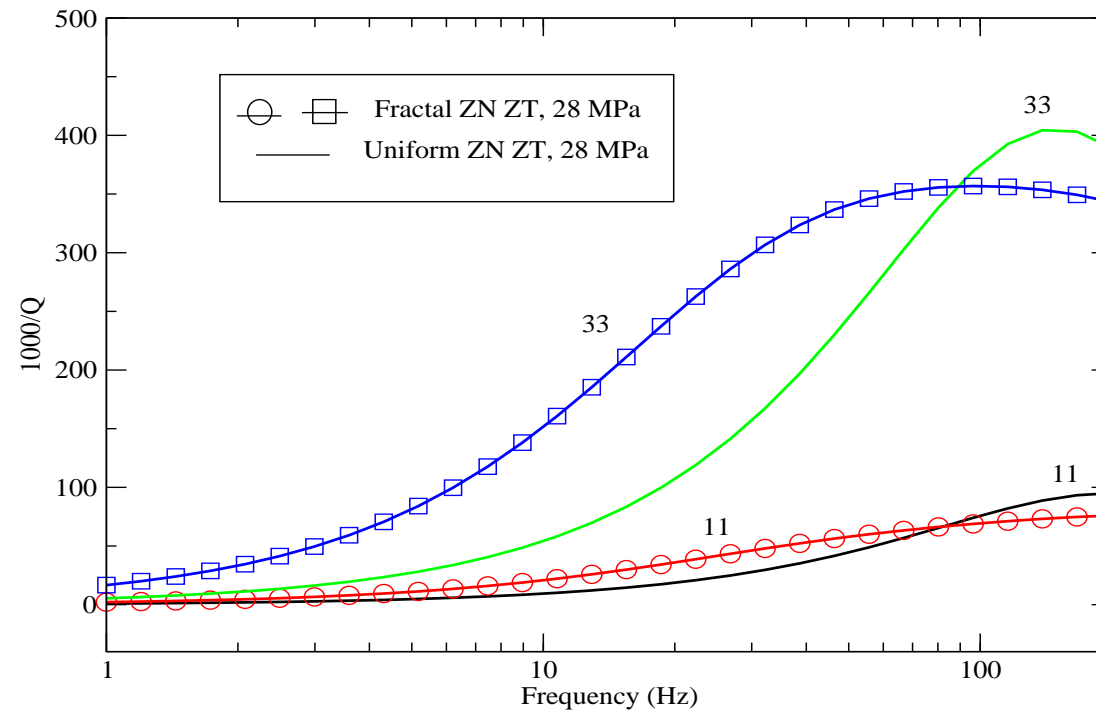
$\sigma = p_c - p_p$ is the effective normal stress, p_c = confining pressure, p_p = pore pressure. “11” and “33” refer to the qP wave along and perpendicular to the fracture plane. Higher pore pressure (circles) implies lower phase velocity. The “33” qP wave is the one more affected by overpressure.



$\sigma = p_c - p_p$ is the effective normal stress, p_c = confining pressure, p_p = pore pressure. “11” and “33” refer to the qP wave along and perpendicular to the fracture plane. Attenuation is stronger in the overpressured case (circles) for “33” waves.



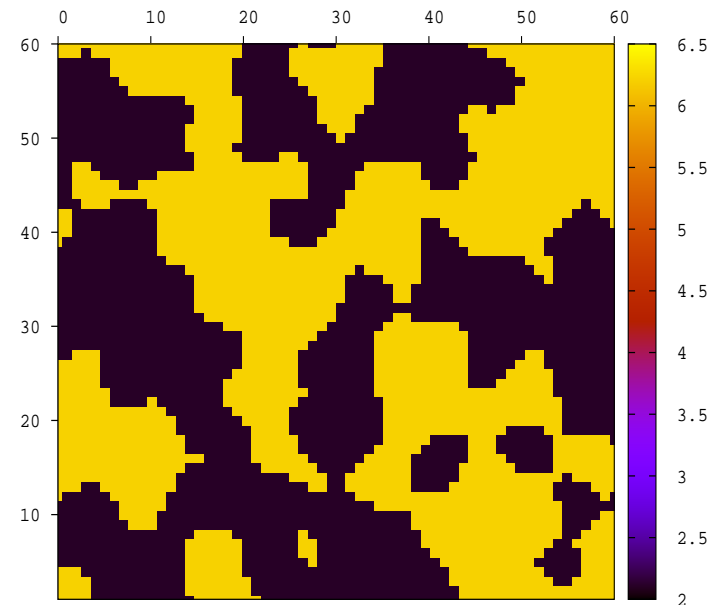
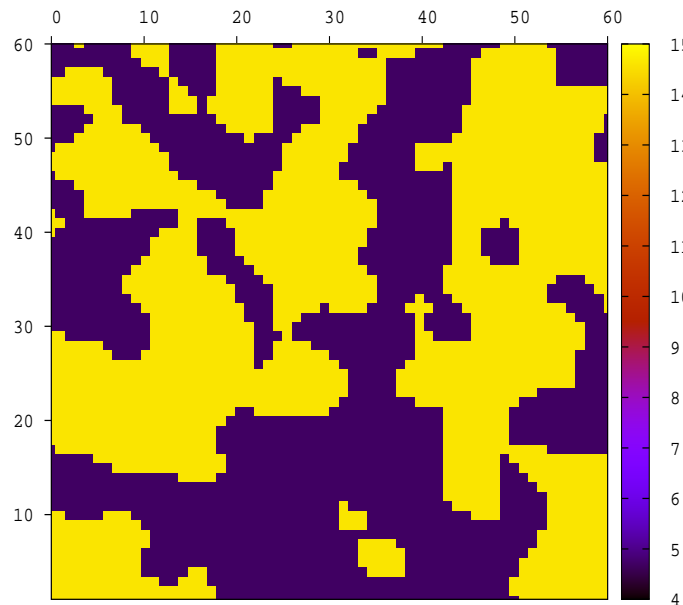
“11” and “33” refer to the qP wave along and perpendicular to the fracture plane. Phase velocities in the fractal case are lower than those obtained with the mean values. The “33” qP wave is the one more affected by the heterogeneities.

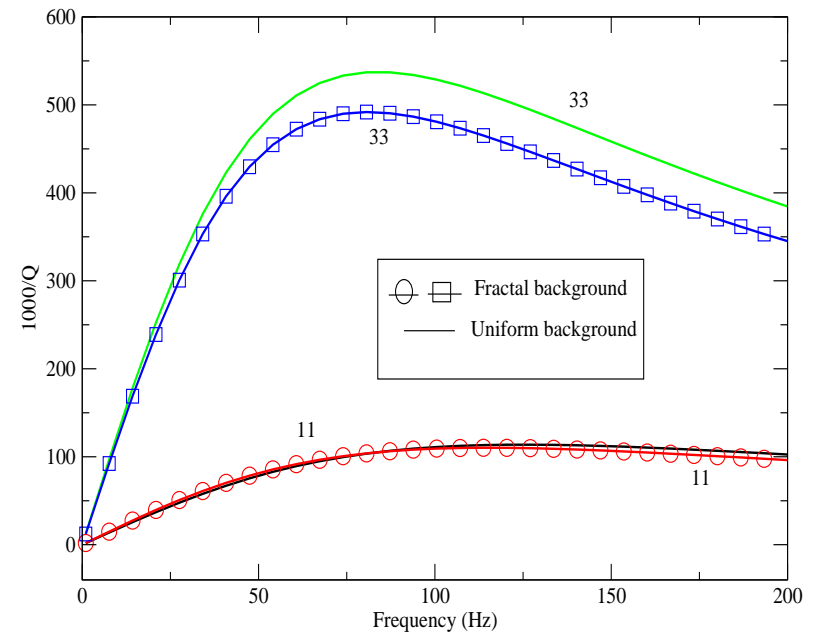
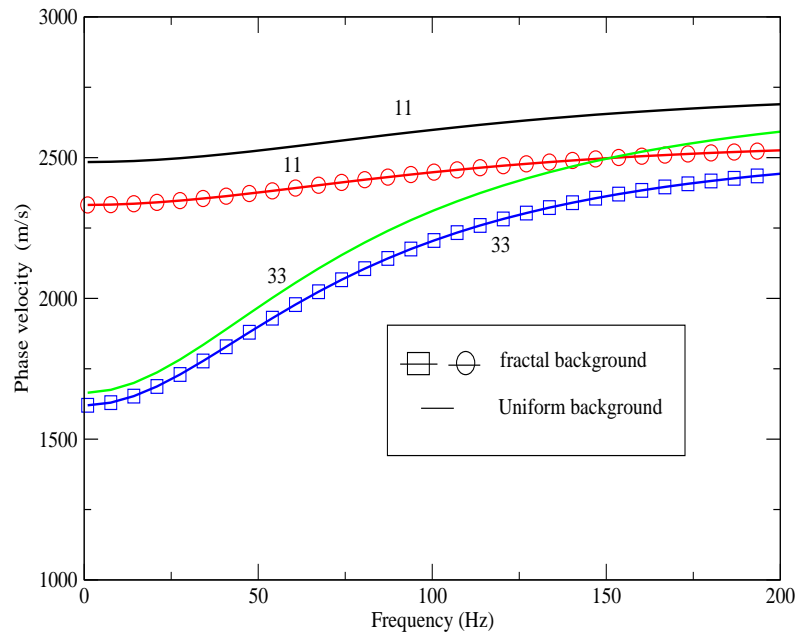


“11” and “33” refer to the qP wave along and perpendicular to the fracture plane. Dissipation factor of the “33” qP wave is more affected by the heterogeneities, showing lower values in the fractal case.

Fractal λ and μ background.

Next we consider 50 % binary fractal variations of the background Lamé constants λ and μ with respect to the mean values 10 GPa and 3.9 GPa, respectively.





“11” and “33” refer to the qP wave along and perpendicular to the fracture plane. Phase velocities are lower for the fractal case for both “11” and “33” qP waves. Concerning attenuation, for qP “33” waves is lower than in the uniform background case, while attenuation for qP “11” waves is not affected by the fractal background.

CONCLUSIONS.

- **Schoenberg's theory** predicts that an homogeneous background containing a dense set of horizontal parallel fractures behaves like a **TIV medium** at long wavelengths.
- We presented a collection of **novel FE harmonic experiments** to test and validate the theory.
- The methodology was applied to a case where there is no analytical solution, such as fractal variations of the fracture compliances at different pore pressures and fractal Lamé parameters.
- In particular, it is shown that **attenuation** can be an **indicator of overpressure** with higher values at high pore pressures.